Experiments in Fluids (2006) 41: 415–424
DOI 10.1007/s00348-006-0169-y

RESEARCH ARTICLE

Xiaochun Shen · Steven L. Ceccio · Marc Perlin

Influence of bubble size on micro-bubble drag reduction

Received: 27 January 2006 / Revised: 25 April 2006 / Accepted: 24 May 2006 / Published online: 23 June 2006

Abstract Micro-bubble drag reduction experiments were conducted in a turbulent water channel flow. Compressed nitrogen was used to force flow through a slot injector located in the plate beneath the boundary layer of the tunnel test section. Gas and bubbly mixtures were injected into a turbulent boundary layer (TBL), and the resulting friction drag was measured downstream of the injector. Injection into tap water, a surfactant solution (Triton X-100, 20 ppm), and a salt-water solution (35 ppt) yielded bubbles of average diameter 476, 322 and 254 μm, respectively. In addition, lipid stabilized gas bubbles (44 μm) were injected into the boundary layer. Thus, bubbles with d^+ values of 200 to 18 were injected. The results indicate that the measured drag reduction by micro-bubbles in a TBL is related strongly to the injected gas volumetric flow rate and the static pressure in the boundary layer, but is essentially independent of the size of the micro-bubbles over the size range tested.

1 Introduction

Micro-bubble drag reduction (MBDR) has been the subject of intense research since the pioneering observation by McCormick and Bhattacharyya (1973). From a physical standpoint, introducing micro-bubbles into the turbulent boundary layer (TBL) of a liquid flow over a solid surface leads to multiple interactions between fluids of different phases and fluid motions with wide ranging scales. Experimental observations of the resulting TBL flow indicate that the injection of bubbles into the TBL can result in the reduction of friction drag downstream of injection. From an engineering perspective, reduced friction drag leads to obvious technological advantages. For example, surface and subsurface vehicles can be designed to cruise at higher speed, with additional economical and environmental benefits. Over the past three decades, accumulated experimental evidence has shown that up to 80% friction drag reduction can be achieved when micro-bubbles are present in the boundary layer of a liquid flow over a solid surface (Merkle and Deutsch 1992; Kodama et al. 2002; Sanders et al. 2006). Although the exact mechanism for MBDR has yet to be identified, it has been demonstrated that bubble-turbulence interaction, bubble deformation, splitting and coalescence, and density and viscosity modification are among the many contributing factors that influence MBDR.

Central to the understanding of MBDR, especially regarding how bubbles modify the momentum and energy transfer in the TBL is the issue of bubble size. Understanding how particles and bubbles affect the velocity fluctuations in fully developed turbulent flow is a subject of significant research. For example, it has been shown that the level of modification by dispersed particles to the energy-containing scales in turbulent flow is strongly correlated with the particle size (Gore and Crowe 1989). Recent experimental (Rensen et al. 2005) as well as direct numerical simulation (DNS) (Ferrante and Elghobashi 2004a) results have demonstrated also a profound influence on the inertial and dissipation scales by either bubbles or dispersed solid particles. However, it is still unclear to what extent such modification influences the friction drag near the wall and whether any particular bubble size is superior to others in reducing friction drag. DNS results of TBLs laden with rigid spherical bubbles (Ferrante and Elghobashi 2004b; Xu et al. 2002) have produced increasing drag reduction with decreasing bubble size, indicating smaller bubbles are more effective in reducing friction drag. Moreover, DNS results of a turbulent channel flow laden with

X. Shen (✉) · S. L. Ceccio · M. Perlin
Department of Mechanical Engineering,
University of Michigan, Ann Arbor, MI 48109, USA
E-mail: xsdl@umich.edu

M. Perlin · S. L. Ceccio
Department of Naval Architecture and Marine Engineering,
University of Michigan, Ann Arbor, MI 48109, USA

deformable bubbles (Lu et al. 2005) also demonstrated substantial drag reduction, suggesting MBDR is related strongly to the modification of the energy-containing scales by larger bubbles. Experimental investigation of the influence of bubble size on MBDR has been limited by the difficulties in varying bubble size, in capturing the bubble trace and size distribution in the TBL, and in measuring the turbulent characteristics in the bubbly TBL.

Although the literature is replete with MBDR experiments, there are only a few experimental efforts that have been devoted to address this issue. In a channel flow experiment with relatively large bubbles and moderate variation in bubble size, it has been observed that the influence of bubble size on the effectiveness of MBDR was insignificant (Moriguchi and Kato 2002). In another flat plate test with a similar variation in bubble size, it was found that larger bubbles tend to remain closer to the solid surface, suggesting MBDR favors larger bubbles (Kawamura et al. 2004). To date, our knowledge of the influence of bubble size on MBDR is incomplete. To understand the influence of bubble size on MBDR, controlled experiments with an extensive variation in bubble size, especially one that is capable of creating very small bubbles, are needed.

In MBDR investigations, bubble size can be characterized by comparing the bubble diameter, d, to the viscous wall unit, l_v ($l_v = v/\sqrt{\tau_w/\rho}$, where v is the fluid kinematic viscosity, τ_w is the wall shear stress, and ρ is the fluid density). In TBL flows, the buffer region spans approximately $5y^+$ to $30y^+$ ($y^+ = y/l_v$, where y is the distance normal to the solid surface) and is the region of high Reynolds stress, turbulent production, and momentum transfer. For bubbles to significantly reduce the wall friction drag, they must interact with the flow structures in this region. While the recent DNS results (Ferrante and Elghobashi 2004b) highlighted a dramatic enhancement in drag reduction by bubbles with $d^+ = 2.4$ ($d^+ = d/l_v$), it has been difficult to produce such flows experimentally. In most MBDR experiments, bubbles are generated by the injection of gas through either a slot injector or a porous plate embedded in a wall. Hence, the bubble size is determined primarily by how the injected gas stream interacts with the local flow structure and is typically two orders of magnitude larger than the wall unit (Merkle and Deutsch 1992; Kodama et al. 2002; Moriguchi and Kato 2002; Sanders et al. 2006; Kawamura et al. 2004). Additionally, MBDR experiments have been conducted by using electrolysis along the wall to generate very small bubbles or out-gassing of bubbles from supersaturated liquids. Using electrolysis, bubbles that are one order of magnitude smaller than those generated through gas injection can be produced. However, large gas phase volume is difficult to achieve. The gas phase volume of the bubbly boundary layer flow is expressed conventionally using the average void fraction, α ($\alpha = Q_a/(Q_a + Q_w)$, where Q_a and Q_w are the gas phase and the liquid phase volumetric flow rate in the boundary layer, respectively). Since it is the near wall gas phase that has the most significant influence on drag reduction and Q_a is measured typically before the gas injection, the void fraction offers only limited physical meaning, although it has been adopted widely as a gross scaling parameter in comparing MBDR results from experiment to experiment. Appreciable reductions in drag are observed when α ranges from 5 to 25%. However, electrolysis and out-gassing produce void fractions that are significantly below 1%.

It is also important to note that while friction drag reduction is sought mostly for the open sea with salt and other surfactants in the aqueous environment, the majority of experiments on MBDR were conducted under laboratory conditions with fresh water. In these experiments, the injected bubble diameters are often on the order of, $d^+ \sim 100$ and thus much larger than the wall unit. However, injection of air into salt or surfactant laden water can yield smaller bubbles. In a recent study, it was found that bubble formation and bubble size distribution vary noticeably under different aqueous conditions (Winkel et al. 2004). In particular, by analyzing bubble images recorded under the same test conditions that included injecting air into fresh tap water, a 20 ppm homogenous surfactant solution, and a saline solution at oceanic salt concentrations (35 ppt), the authors found that the average bubble size was reduced by a factor of 2 in the surfactant solution and by a factor of 4 in saltwater. If reduced bubble size is indeed favorable for MBDR, one would expect that due to the formation of smaller bubbles, for the same gas injection rate, increased drag reduction would be observed when surfactant or salt exists in the aqueous environment.

In the present study, we address the influence of bubble size on MBDR. Using several approaches, the bubble size is varied by one order of magnitude in our experiments. First, bubbles are generated by injecting compressed nitrogen into different aqueous environments to examine the influence of salt and surfactant on the resulting bubble size and drag reduction. Next, we adopted a method used in medical applications to produce lipid-stabilized air bubbles that are one order of magnitude smaller than those generated through gas injection. Such bubbles are then injected into the TBL to measure the drag reduction with smaller bubbles. While the smallest bubble tested is still one order of magnitude larger than the wall unit, the present measurements expand our limited database on the influence of bubble size on MBDR as our d^+ varied from 200 to 18.

2 Experimental apparatus and procedures

2.1 Test facility

The high-speed re-circulating water tunnel used in this experimental study is located in the Marine Hydrodynamics Laboratory at the University of Michigan. This water tunnel, as shown schematically in Fig. 1, is a 1/14

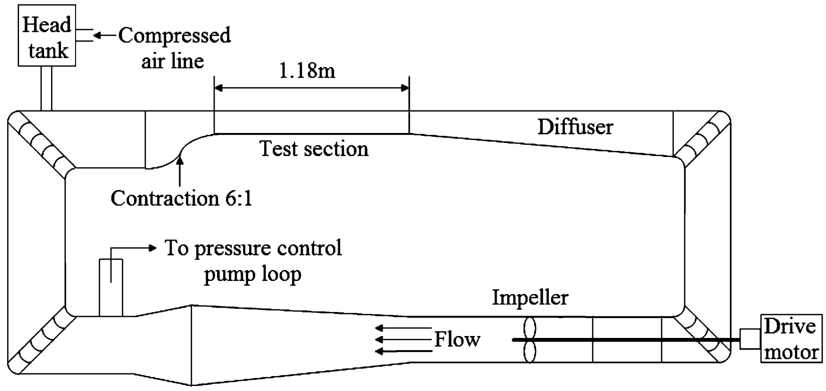

Fig. 1 Schematic of the high-speed re-circulating water tunnel

scale model of the U.S. Navy's William B. Morgan Large Cavitation Channel in Memphis, Tennessee. The water tunnel includes a 6:1 contraction section, followed by a 1.18 m (length) × 0.22 m × 0.22 m (width and height) square test section with 45° corner fairings, and a 1.85 m long diffuser section. The impeller that drives the flow is powered by a 149 kW electric motor, leading to a maximum test section centerline velocity of 22 m/s and a Reynolds number as high as 4.8×10^6 based on the tunnel width. The tunnel volume capacity is approximately 2,900 l, determined by solid geometry and verified with conductivity tests after known quantities of salt (i.e., Instant Ocean) were dissolved in the tunnel water.

A pressurized head tank is used to set the test section static pressure, allowing the test section static pressure to be adjusted from atmospheric pressure to 700 kPa. However, with liquid or gas injection, the static pressure of the tunnel rises and hence may contaminate the drag reduction results (see Fig. 9). To compensate for the pressure increase due to injection, an open-loop pressure control system is implemented whereby a constant flux of fluids, determined by trial and error during each injection test, is pumped from the tunnel so that the test section static pressure remains nearly constant. The fluids drained are stored in an external holding tank and returned to the tunnel between runs.

In the middle of the test section window of the water tunnel, a 812.8 mm (length) × 152.4 mm (width) precision-machined stainless-steel test window is mounted using both the plate-on-top and plate-on-bottom orientations (Fig. 2). A 101.6 mm (length) × 139.7 mm (width) gas injector, made of yellow brass, is located 152.4 mm from the leading edge of the test plate. The injection slot is a 0.5-mm gap and is inclined 15° to the wall. The slot is located 76.2 mm from the upstream edge of the injector. A schematic of the cross-section of the injector is shown in Fig. 3. Downstream of the injector, two 50 mm circular fused-silica glass windows facilitated optical access for imaging the bubbly layer adjacent to the tunnel wall. These two observation windows, as shown in Fig. 2, are separated by 254 mm with windows A and B located 76.2 and 300.2 mm downstream of the injector slot, respectively. Further downstream of the observation windows, a rectangular floating element force balance is located 457.2 mm from the injection slot and is used to measure directly the wall friction force. The floating plate's dimensions are 152.4 mm (length) × 101.6 mm (width). The gas injector, the observation windows and the floating surface of the force balance are all centered spanwise on the test plate.

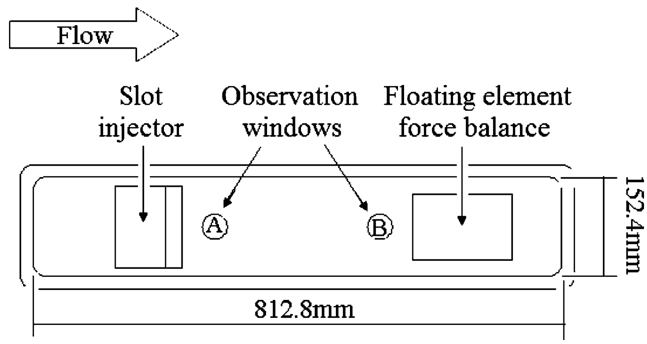

Fig. 2 Schematic of the upper/lower test window portion of the test section as viewed from within the tunnel

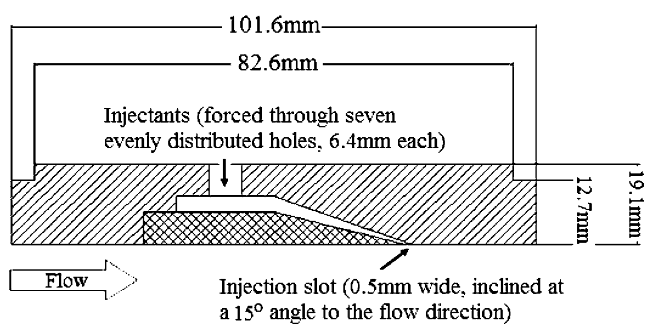

Fig. 3 Cross-section schematic of the injector. Compressed nitrogen and lipid bubbles are forced through the injector by a manifold with seven evenly distributed ports in the cross-stream direction

2.2 Experimental conditions

To change the bubble size by at least one order of magnitude, two types of micro-bubble drag reduction tests are conducted. First, three sets of drag reduction experiments are performed with compressed nitrogen injected through the slot injector into: (1) fresh tap water; (2) a uniform 20 ppm surfactant solution (Triton-X-100, Union Carbide); (3) a uniform 35 ppt saltwater (Instant Ocean, Aquarium Systems). Both a plate-on-top (where buoyancy moves the bubbles toward the plate surface) and a plate-on bottom orientation (where buoyancy moves the bubbles from the plate surface) are tested. The injection rate is varied from 30 to 180 standard liters per minute with the channel absolute static pressure maintained at 100 ± 10 and 200 ± 10 kPa, respectively. For the plate-on-top orientation, tests are conducted also in tap water with the injection rate fixed at 60 standard liters per minute when the channel absolute static pressure is varied from 70 to 240 kPa. In these experiments, the bubble size is determined primarily by the interaction between the injected gas and the flow characteristics in the boundary layer. The average bubble size is typically on the order of several hundred microns.

In the second test category, micron-sized bubbles that are coated with monolayer lipids (Phosphatidylcholine 90%, DNP International) and emulsifier (PEG-40, Sigma) are produced following the procedures outlined in Borden and Longo (2002). The water, lipid and emulsifier mixture is sonicated with a Sonics VC-750 ultrasonic processor to produce stable micro-bubbles. The amount of gas carried by the lipid-stabilized micron-sized bubbles is estimated from the difference in volume of the mixture before and after sonication by assuming that the monolayer micro-bubbles are spherical, and have a perfect packing density of 74%. The mass flow rate of the bubbly mixture is measured by recording the change in weight of the lipid filled container as a function of time. The diameter of the lipid-stabilized micro-bubbles is one order of magnitude smaller than the bubbles generated through gas injection and is independent of the flow condition in the boundary layer.

To determine the influence of surfactant, salt, and lipid bubbles on the viscosity of the fluids in the channel, samples of the test fluids are drained from the channel during each drag reduction experiment. The samples are then fed by gravity through a 1.1-cm horizontal smooth copper pipe. The pipe is 3 m long, consists of two pressure taps separated by 2 m, with the upstream pressure tap located 0.5 m from the pipe inlet. The flow rate in the pipe is varied by changing the pressure head upstream and monitored at the pipe outlet. The pressure difference is measured by a U-tube manometer with an error of ±2 mm H_2O. The Fanning friction coefficient, f ($f = \frac{\Delta P}{L}\frac{D}{2\rho U^2}$, where ΔP is the measured pressure drop; L is the distance between the pressure taps; D is the pipe diameter; ρ is the density of the fluids; and U is the average speed in the pipe), measured in the pipe test is shown in Fig. 4. Also shown is the Prandtl–Karman Fanning friction coefficient curve for smooth pipe flow as given by

$$1/\sqrt{f} = 4\log_{10}(\boldsymbol{Re}_d\sqrt{f}) - 0.4 \quad (1)$$

These results indicate that the addition of surfactant, salt, or lipid bubbles does not noticeably change the viscosity of the circulating fluids in the channel.

For all results reported, the water tunnel is operated at a fixed test section free-stream speed of 11.1 m/s. Before each nitrogen injection experiment, the channel is circulated for a minimum of 10 min at a relatively low speed to purge air from the tunnel free-stream and to ensure uniform mixing of either the surfactant or salt. For the lipid bubble experiments, prior to the drag reduction test, the channel is also circulated at low speed to remove the residual gas in the tunnel. After each drag reduction test, the channel is drained completely and refilled with fresh tap water prior to the next test.

2.3 Instrumentation

For the nitrogen injection test, the injection rate was monitored continuously with an Omega FMA-1600A mass and volumetric flow meter. This flow meter offers a rated full scale accuracy of ±1% at standard conditions. During a test, the injection pressure is maintained at a constant level by using two pressure regulators upstream of the flow meter. For the lipid bubble tests, the weight of the container that holds the bubbly lipid solution is measured by a SensoTec model 41 "pancake" load cell. To determine the basic flow character over the test section window, a United Sensor USNH-A-336 pitot tube is used to measure the mean velocity distribution of the single-phase flow at the location of the injection slot and the center of the floating element force balance. For this measurement, an aluminum test window, with mounting holes for the pitot tube probe only, replaced the stainless-steel test window.

A Sony XC-55BB progressive-scan black-white video camera module, connected to a Nikon AF Micro

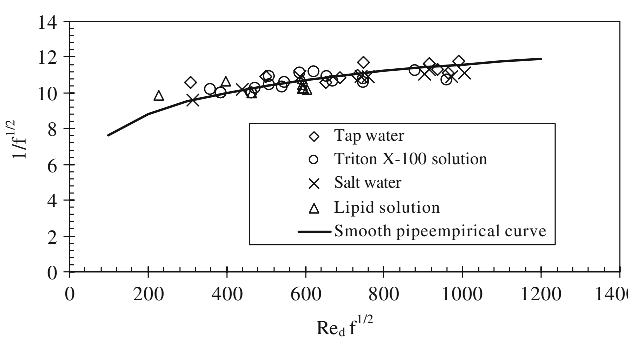

Fig. 4 Fanning friction coefficient from pipe experiments of fluids viscosity

Nikkor 105 mm lens through a C-mount adaptor, is used to acquire images of the bubbly boundary layer through the observation windows, A and B. The video camera has a resolution of 659 × 494 pixels. For the nitrogen only injection tests, the camera's viewing area spanned approximately 12 mm in the stream-wise direction and 9 mm in the cross-stream direction, corresponding to a pixel resolution of approximately 18 μm/pixel. For the lipid bubble tests, to capture smaller bubbles, the camera's viewing area is reduced to approximately one-fourth of that in the gas injection tests. The pixel resolution is approximately 4.8 μm/pixel. The frame rate and shutter speed of the camera, fixed at 5 Hz and 10 μs respectively, are controlled by an external trigger signal produced by a Stanford DG535 delay generator. The bubbly layer is illuminated with incandescent light sources shone through the other three transparent windows of the test section. Bubble images are acquired with a Bit-Flow RAV-PCI-110-VNS frame grabber.

Skin-friction drag is measured directly with a floating element force balance. The rectangular floating element is mounted on a custom beryllium–copper load cell that uses semi-conductor strain-gages for high accuracy, and is precisely leveled and made flush with the test section window. The gap around the sensor is adjusted approximately to 50 μm on each side. The drag balance is dry calibrated by applying loads ranging from 0.9 to 7.2 N to the center of the floating plate in the flow direction. The response of the force balance exhibited excellent linearity over the range of the loads tested. An Omega PX-603 pressure transducer was placed inside the floating plate housing to monitor the channel static pressure. Output from this pressure sensor is used to guide the pressure control pump and correct excursions from the desired tunnel pressure. During a test, signals from the skin-friction balance, the pressure transducer, and the gas flow meter or the load cell are sampled simultaneously at 100 Hz. Mean physical quantities are inferred from statistics of the electrical signals. An example of the typical time series from the force balance, the flow meter, and the pressure transducer is presented in Fig. 5.

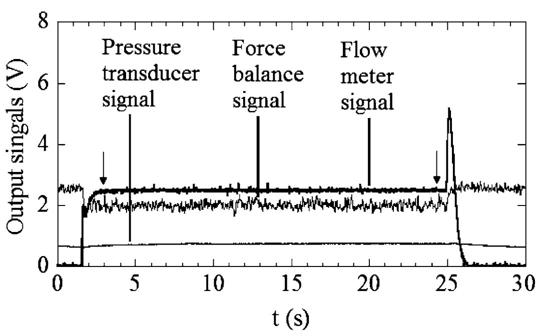

Fig. 5 Sample output from the instruments. The *arrows* indicate the range over which the mean physical statistics are calculated

3 Results

3.1 Single-phase flow

The mean velocity in the boundary layer is measured with a pitot tube probe for both the plate-on-top and plate-on-bottom orientations. The measurements are performed at the locations of the injection slot and the center of the floating element force balance. The results are shown in Fig. 6. The 1/7th power-law (White 1999)

$$\frac{u(y)}{U_\infty} = \left(\frac{y}{\delta_{99}}\right)^{1/7} \tag{2}$$

provides an excellent fit to the measured velocity profiles. The 99% thickness, δ_{99}, of the boundary layer is determined from the measured velocity distributions. The boundary layer displacement thickness, δ^*, is inferred from the 1/7th power-law. The volumetric water flow rate in the boundary layer at the position of the injection slot is determined from:

$$Q_{\mathrm{w}} = U_\infty(\delta_{99} - \delta^*)b, \tag{3}$$

where b = 184 mm is the width of the test section 17 mm above the window surface (the average width of the channel over the chamfered section), and U_∞ is the free-stream velocity. The viscous wall unit, l_v, is determined based on the measured average drag force over the surface of the friction force balance. Some basic properties of the single-phase boundary layer flow are listed in Table 1.

Prior to the bubble drag reduction test, the average friction force is measured for the plate-on-top orientation with tap water circulating in the channel. The measured single-phase friction coefficient, C_{FO}, is shown in Fig. 7. These results agrees well with the friction law

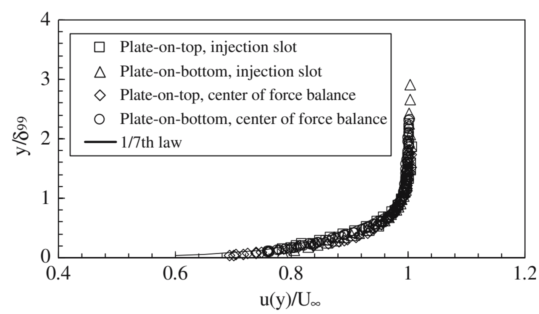

Fig. 6 Mean velocity distribution in the boundary layer

Table 1 Basic properties of the single-phase turbulent boundary layer flow

U_∞ (m/s)	δ_{99} (mm)	δ^* (mm)	Q_{w} (m^3/s)	C_{FO} (×10^3)	l_v (μm)
11.1	10.5	1.3	0.018	0.027	2.4

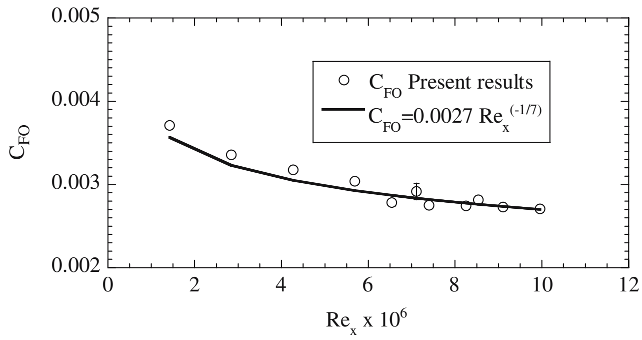

Fig. 7 Single-phase wall friction coefficient measured by the floating element force balance. Also shown is the 3% error bar

derived from the mean velocity distribution based on (2), i.e., $C_{FO} = 0.027Re_x{}^{(-1/7)}$, also shown in Fig. 7. At 11.1 m/s, the uncertainty associated with the measured wall friction force is approximately 3% of the average force balance output, based on results from over 100 independent single-phase tests. When salt or surfactant is added to the tunnel fluid, the measured single-phase friction coefficients are nearly identical to that of tap water. This, together with the pipe test results in Fig. 4, indicates that under the additive concentration tested, the surfactant and salt acted as passive scalars, changing only the surface tension of the gas–liquid interface when nitrogen gas is present.

3.2 Bubble images and bubble size distributions

During each drag reduction test, bubble images are recorded with the camera focused at the interior wall of observation window B upstream of the friction force balance. To accurately determine the bubble size, a Canny edge detector algorithm (Canny 1986) is implemented to find the boundaries of the captured bubbles in each image. The size of each bubble is then determined by measuring the maximum horizontal or vertical distance between the bubble boundaries based on the edge detection results. Overlapped bubbles and bubbles without clearly defined edges are not included in the bubble size analysis. Using this method, the measured bubble size is accurate to ±1 pixel, i.e., ±18 μm for the bubbles formed during nitrogen injection and ±4.8 μm for the lipid bubbles. To determine the bubble size distribution, 1,500 bubbles are counted from each set of drag reduction images.

Typical examples of the bubble images and the bubble size histograms under each test condition are presented in Fig. 8. Here, only the results from the observation window adjacent to the force balance are reported. The depth of field is relatively large (>2 mm). Therefore, the images capture bubbles both near and relatively far from the wall, and reveal the overall bubble size populations. For the nitrogen injection tests shown in Fig. 8, the bubble images are acquired with the channel static pressure maintained at 200 ± 10 kPa and the injection rate fixed at 0.001 m^3/s. Note that a different injection rate and static pressure would possibly alter these bubble size distributions. The average diameter of the bubbles formed in tap water is 476 μm. In the 20 ppm Triton X-100 solution, the mean diameter is reduced to approximately 322 μm. With the addition of sea salt (35 ppt), the mean bubble diameter is reduced further to approximately 254 μm. The histograms of the bubble sizes are in qualitative agreement with the findings in Winkel et al. (2004). However, at similar surfactant or salt concentration, the measured mean bubble diameters in the present study are noticeably larger than the results in Winkel et al. (2004). The differences are associated primarily with the differences in the injectors used in the two tests and the downstream locations at which the bubble images are recorded. In Winkel et al. (2004), the tunnel freestream speed was 16 m/s and the tunnel-width-based Reynolds number was 4.1×10^6, but more importantly, air was injected through a sintered metal injector and the bubble images were acquired immediately (55 mm) downstream of the gas injector. In the present study, a slot injector is used and the bubble images are recorded 300 mm from the gas injector. Hence in the current study, the bubble size distribution is different from Winkel et al. (2004) and the bubbles may be subject to stronger coalescence. Lipid-stabilized bubble images are acquired when the channel static pressure is maintained at 100 ± 10 kPa. Likewise, the size of the lipid-stabilized micro-bubbles does not change significantly with channel pressure due to the lipid "shell" that coats the gas core. The mean diameter of the lipid-stabilized air bubbles is approximately 44 μm. Some basic statistics of the bubble sizes are summarized in Table 2. When non-dimensionalized by the viscous wall units, l_ν, these results correspond to a variation in the non-dimensionalized mean bubble diameter from $d^+ \sim 200$ to $d^+ \sim 18$.

3.3 MBDR with nitrogen injection

In MBDR studies, it is meaningful to compare drag reduction results based on the mean void fraction, α, throughout the boundary layer. In fact, various approaches have been proposed in the literature to test whether certain universal features exist when the fraction of drag reduction is presented as a function of the void fraction (Merkle and Deutsch 1992; Kodama et al. 2002). However, it is important to note that the injected gas volumetric flow rate depends strongly on the static pressure of the test section. In Fig. 9, drag reduction results for tap water with nitrogen injection using the plate-on-top orientation is presented as a function of the static pressure in the test section. The injection rate is fixed at 0.001 m^3/s, measured at standard pressure and temperature. The magnitude of drag reduction, given as C_F/C_{FO}, is shown in Fig. 9 as a function P/P_O, where C_F is the skin-friction coefficient during gas injection; P is

Fig. 8 Sample bubble images and bubble size distributions for various bubble drag reduction experiments. The distance between the crosses at the bottom of each bubble image is 1,411 μm, from which the pixel resolution and the field of view for each image are determined. For the nitrogen injection results, the images are acquired with the channel static pressure maintained at 200 ± 10 kPa and the injection rate fixed at 0.001 m^3/s. **a** Nitrogen injection into tap water, plate-on-bottom. **b** Nitrogen injection into Triton X-100 solution (20 ppm), plate-on-bottom. **c** Nitrogen injection into saltwater (35 ppt), plate-on-bottom. **d** Lipid bubble image, plate-on-top

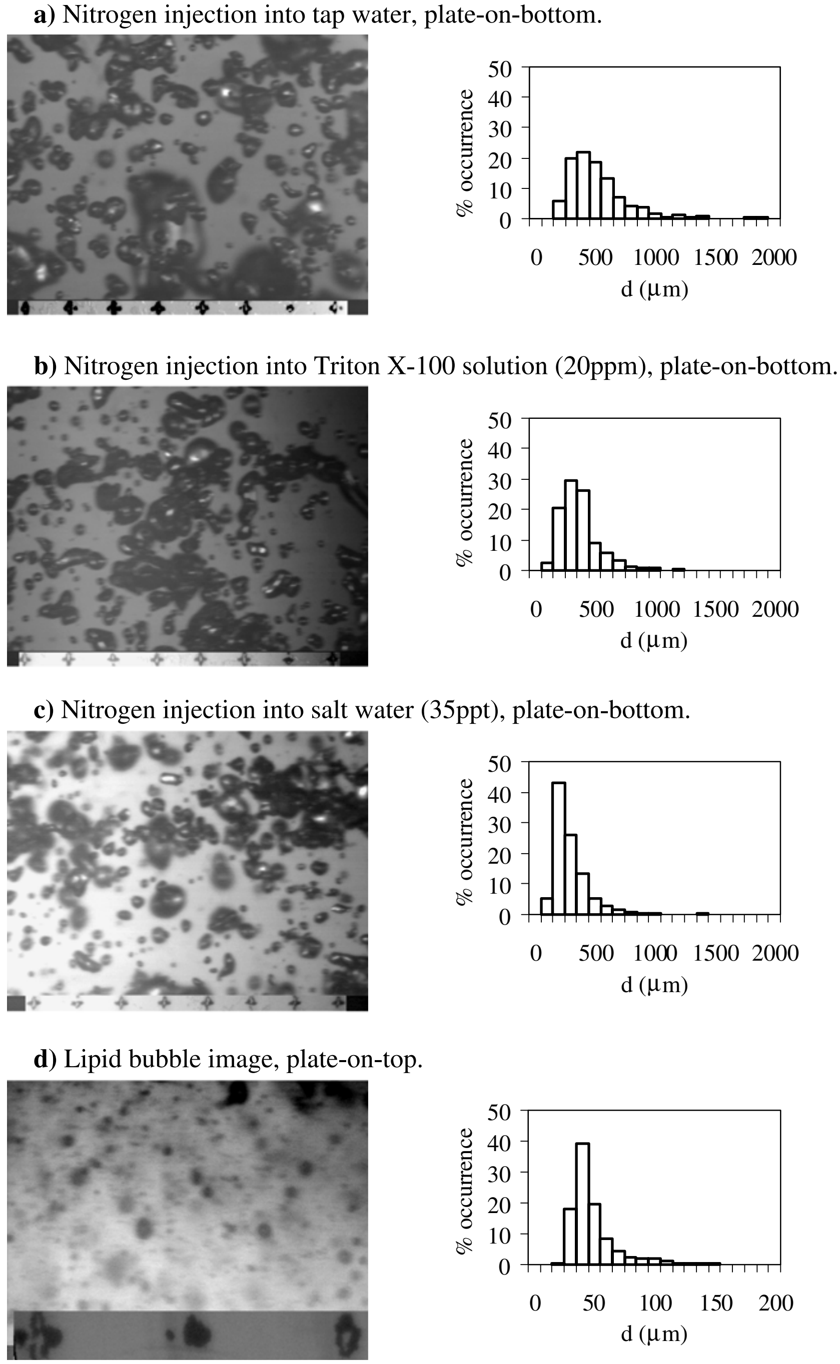

Table 2 Basic properties of the bubble size for each drag reduction experiment

	Mean (μm)	Median (μm)	$d^+ = d_{\mathrm{Mean}}/l_v$
Water nitrogen injection	476	411	200
20 ppm Triton X-100 nitrogen injection	322	295	134
35 ppt Saltwater nitrogen injection	254	209	106
Lipid bubble injection	44	37	18

the static pressure in the test section and P_O is atmospheric pressure. With a constant gas volumetric inflow rate, as the channel static pressure is increased from 70 to 240 kPa, C_F/C_{FO} spans 0.84–0.96, showing less drag reduction with increased pressure at the same injection rate. Increasing the static pressure causes the volumetric flow rate of the injected gas phase to decrease proportionally. These results show that when using void fraction to compare MBDR results, the gas volumetric inflow rate must be corrected for the static pressure in the test section. They also indicate that while MBDR

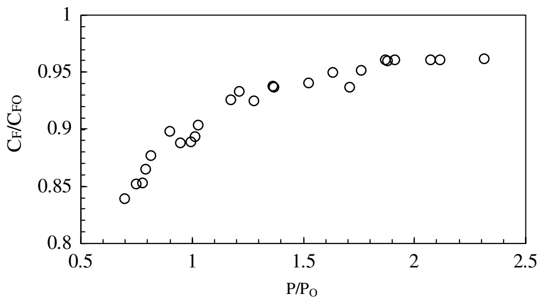

Fig. 9 Effects of static pressure on friction drag reduction. Tap water with nitrogen injection, plate-on-top. The injection rate is fixed at $Q_a = 0.001\ m^3/s$. $P_O = 101$ kPa

could be a potential drag reduction technique for surface vessels, the efficiency of drag reduction would decrease significantly with increasing depth if all other parameters held constant.

Friction drag data with nitrogen injection in tap water are collected using both the plate-on-top and plate-on-bottom orientations. For the plate-on-top configuration, the channel pressure was maintained at both 100 ± 10 and 200 ± 10 kPa with the volumetric gas flow rate varied from 30 to 180 standard liters per minute. For the plate-on-bottom orientation, only the higher-pressure condition is tested. The results are shown in Fig. 10. Besides the well-established trend of increased drag reduction with increased injection rate, under similar test conditions (i.e., 200 kPa), there is no observable difference between the drag reduction results from the two plate orientations at the test speed examined here. At a free-stream speed of 11.1 m/s, the influence of buoyancy is not expected to be significant. Thus, the difference between the two sets of drag reduction results under different plate orientation, both collected at 200 kPa, is expected to be small, in good agreement with the experimental data. For the plate-on-top orientation, the fraction of drag reduction at 200 kPa is noticeably smaller than the fraction of drag reduction at 100 kPa and the same injection rate. When Q_a is $0.001\ m^3/s$, these results are in quantitative agreement with the results shown in Fig. 9.

Figures 11 and 12 present the drag reduction results with nitrogen injection into a 20 ppm Triton X-100 solution and a 35 ppt sea salt solution, respectively. The test conditions are the same as those in Fig. 10 for tap water with gas injection. While the lower pressure surfactant solution and saltwater yield similar fractions of drag reduction as the lower pressure tap water tests, the higher-pressure drag reduction results are also in good agreement with the tap water drag reduction results for both plate orientations. Based on the viscous wall unit determined from the single-phase flow, the average bubble size in tap water corresponds to $200d^+$. With the addition of surfactant and salt, the mean bubble size is reduced to $134d^+$ and $106d^+$, respectively. The data from these tests indicate that changing the aqueous environment, consequently changing the surface tension between the liquid–gas interface, and hence the size of the bubbles formed during gas injection, essentially has no influence on the measured fraction of drag reduction. This is consistent with the observation made in a MBDR test with an axisymmetric body immersed in homogenous surfactant (Aerosol OT) solutions (Fontaine et al. 1999).

During each nitrogen injection drag reduction experiment, the injection rate is measured at standard conditions. However, at any injection rate, the gas phase volumetric flow rate in the boundary layer depends on the pressure of the water channel. When the measured injection rate is converted to a volumetric flow rate under the channel static pressure according to the ideal gas law, and the void fraction calculated using (3), the drag reduction results in Figs. 10, 11 and 12 are re-examined as a function of the calculated void fraction. The results are presented in Fig. 13. The collapse of the results with nitrogen injected in tap water, surfactant solution and saltwater, at both 200 and 100 kPa, suggests that it is the gas phase volumetric flow rate in the boundary layer (influenced both by the free-stream pressure and injection rate) that exerts the most influence on the measured fraction of drag reduction.

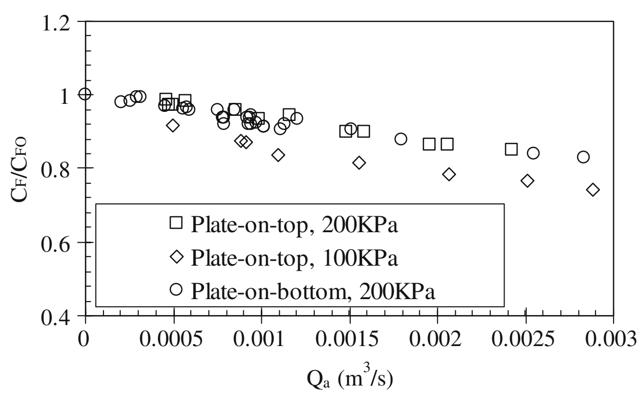

Fig. 10 Fraction of drag reduction as a function of the injection rate with tap water

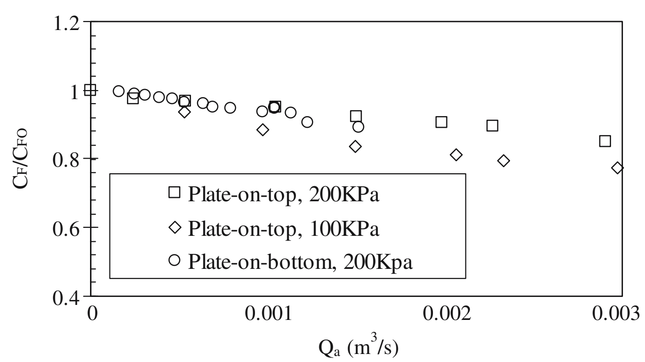

Fig. 11 Fraction of drag reduction as a function of the injection rate with 20 ppm Triton X-100 solution

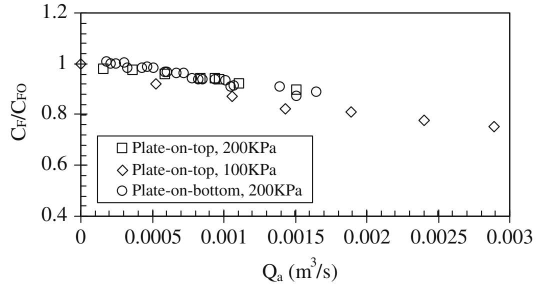

Fig. 12 Fraction of drag reduction as a function of the injection rate with 35 ppt saltwater

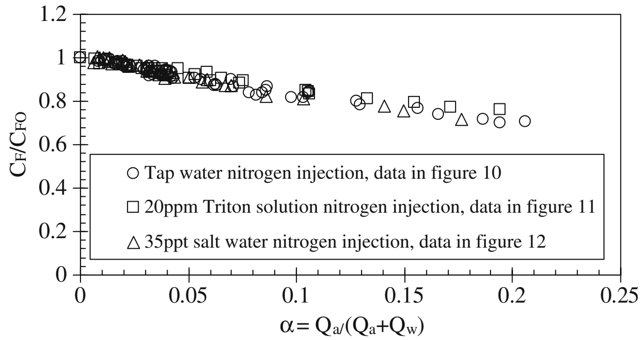

Fig. 13 Fraction of drag reduction as a function of the void fraction for all the nitrogen injection results

3.4 MBDR with lipid bubble injection

Drag reduction results with the injection of lipid-stabilized micro-bubbles, and the results from injecting nitrogen into tap water, are shown in Fig. 14. For the lipid bubble injection experiments, both the plate-on-top and plate-on-bottom orientation are employed. The channel static pressure is set at either 200 or 100 kPa. Due to the difficulties in producing such small bubbles, only low gas-phase volumetric flow rates are available. The measured lipid bubble size corresponds to $18d^+$, at least an order of magnitude smaller than the bubbles formed by nitrogen injection into fresh water. Since such bubbles are stabilized by lipid shells, the gas phase volume carried by these lipid bubbles does not change significantly with channel pressure. The difference in the level of drag reduction produced by these much smaller bubbles is marginal and is essentially the same as the injection of an equivalent volumetric flow rate of much larger bubbles.

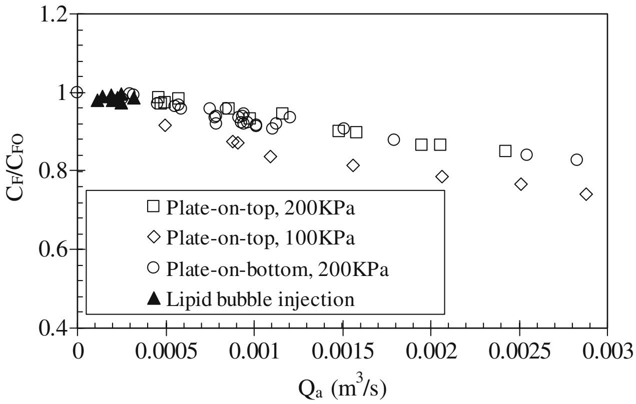

Fig. 14 Fraction of drag reduction with lipid bubble injection compared to nitrogen injection results in tap water

4 Conclusion

Friction drag reduction using micro-bubbles in a high-speed water channel flow is studied experimentally, focusing on the influence of bubble size on the effectiveness of MBDR. The wall friction force is measured directly using a floating element force balance for both the single-phase flow and the bubbly flow. The bubble size is determined from photographic imaging. In the nitrogen injection test, the bubble size is varied from 476 μm in fresh water, to 322 μm in a 20 ppm Triton X-100 solution, to 254 μm in a 35 ppt saltwater solution. It is found that the most important parameter in determining the fraction of drag reduction during gas injection is the effective gas phase volumetric flow rate, which is influenced both by the injection rate and the static pressure under the test conditions. Drag reduction experiments are conducted also with lipid-stabilized gas bubbles. During the lipid bubble drag reduction tests, the average bubble size is further reduced to 44 μm. However, such bubbles produced essentially the same level of drag reduction as the bubbles that are at least one order of magnitude larger at an equivalent volumetric flow rate. These results indicate that drag reduction is related strongly to the injected gas volumetric flow rate and the static pressure in the boundary layer. Changing bubble size had essentially no influence on the measured friction drag, at least over the range of $18 \leq d^+ \leq 200$, suggesting that the magnitude of drag reduction using micro-bubbles is not a strong function of bubble size.

The strong influence of volume flux on the level of MBDR suggests that it is the change in density in the near wall region that may be largely responsible for the MBDR effect. Turbulence-bubble interaction at the smallest scales may become increasingly important if bubbles with $d^+ \sim 1$ could be produced and injected in quantity into the TBL. However, for practical applications of MBDR, these bubbles would be on the order of 1 μm in diameter, and no economic method currently exists whereby sufficient volumes of these bubbles can be produced to achieve the necessary void fraction for meaningful MBDR to occur.

Acknowledgements This work was sponsored by the Office of Naval Research, Dr. Patrick Purtell, Program Manager, under ONR contract number N0014-01-1-0880. The authors would like to thank Prof. M. Longo of the University of California at Davis, for her help in creating the lipid coated microbubbles.

References

Borden M, Longo M (2002) Dissolution behavior of lipid monolayer-coated, air-filled microbubbles: effect of lipid hydrophobic chain length. Langmuir 18:9225–9233

Canny J (1986) A computational approach to edge detection. IEEE Trans Pattern Anal Mach Intell 8:679–698

Ferrante A, Elghobashi S (2004a) On the physical mechanisms of two-way coupling in particle-laden isotropic turbulence. Phys Fluids 15:315–329

Ferrante A, Elghobashi S (2004b) On the physical mechanisms of drag reduction in a spatially developing turbulent boundary layer laden with microbubbles. J Fluid Mech 503:345–355

Fontaine AA, Deutsch S, Brungart TA, Petrie HL, Fenstermacker M (1999) Drag reduction by coupled systems: microbubble injection with homogeneous polymer and surfactant solutions. Exp Fluids 26:397–403

Gore RA, Crowe CT (1989) Effect of particle size on modulating turbulent intensity. Int J Multiphase Flow 15:279–285

Kawamura T, Fujiwara A, Takahashi T, Kato H, Matsumoto Y, Kodama Y (2004) The effects of the bubble size on bubble the dispersion and skin friction reduction. In: Proceedings of the 5th symposium on smart control of turbulence, Tokyo, pp 145–151

Kodama Y, Kakugawa A, Takahashi T, Nagaya S, Sugiyama K, SR239 Committee (2002) Microbubbles: drag reduction mechanism and applicability to ships. In: Proceedings of the 24th symposium on naval hydrodynamics, Fukuoka, pp 1–20

Lu J, Fernandez A, Tryggvason G (2005) The effect of bubbles on the wall drag in a turbulent channel flow. Phys Fluids 17:095102

McCormick ME, Bhattacharyya R (1973) Drag reduction of a submersible hull by electrolysis. Nav Eng J 85:11–16

Merkle CL, Deutsch S (1992) Microbubble drag reduction in liquid turbulent boundary layers. Appl Mech Rev 45(3):103–127

Moriguchi Y, Kato H (2002) Influence of microbubble diameter and distribution on frictional resistance reduction. J Mar Sci Technol 7:79–85

Rensen J, Luther S, Lohse D (2005) The effect of bubbles on developed turbulence. J Fluid Mech 538:153–187

Sanders WC, Winkel EW, Dowling DR, Perlin M, Ceccio SL (2006) Bubble friction drag reduction in a high Reynolds number flat plate turbulent boundary layer. J Fluid Mech 552:353–380

White FM (1999) Fluid mechanics, 4th edn. McGraw-Hill, New York

Winkel ES, Ceccio SL, Dowling DR, Perlin M (2004) Bubble-size distributions produced by wall injection of air into flowing freshwater, saltwater and surfactant solutions. Exp Fluids 37:802–810

Xu J, Maxey MR, Karniadakis GE (2002) Numerical simulation of turbulent drag reduction using micro-bubbles. J Fluid Mech 468:271–281